Endothelial Rbpj is essential for the education of tumour-associated macrophages

Ronja Mülfarth[1,2*], Elisenda Alsina-Sanchis[1*], Iris Moll[1], Sarah Böhn[1], Lena Wiedmann[1,2,] Lorea Jordana[1], Tara Ziegelbauer[1], Jacqueline Taylor[1], Francesca De Angelis Rigotti[1,3], Adrian Stögbauer[1], Benedetto Daniele Giaimo[4], Adelheid Cerwenka[5,6], Tilman Borggrefe[4], Andreas Fischer[1,5,7,*], Juan Rodriguez-Vita[1,3,*]

[1]Division Vascular Signaling and Cancer, German Cancer Research Center (DKFZ), 69120 Heidelberg, Germany.

[2]Faculty of Biosciences, University of Heidelberg, 69120 Heidelberg, Germany.

[3]Tumour-Stroma Communication Laboratory, Centro de Investigación Príncipe Felipe, 46012 Valencia, Spain.

[4]Institute of Biochemistry, University of Giessen, 35392 Giessen, Germany.

[5]European Center for Angioscience (ECAS), Medical Faculty Mannheim, University of Heidelberg, 68167 Mannheim, Germany.

[6]Department of Immunobiochemistry, Mannheim Institute for Innate Immunoscience (MI3), Medical Faculty Mannheim, University of Heidelberg, 68167 Mannheim, Germany

[7]Institute for Clinical Chemistry, University Medical Center Göttingen, 37075 Göttingen, Germany.

* Equal contribution.

Correspondence to: a.fischer@dkfz.de, jrodriguez@cipf.es

Abstract

Epithelial ovarian cancer (EOC) is one of the most lethal gynaecological cancers worldwide. EOC cells educate tumour-associated macrophages (TAMs) through CD44-mediated cholesterol depletion to generate an immunosuppressive tumour microenvironment (TME). In addition, tumour cells frequently activate Notch1 receptors on endothelial cells (ECs) to facilitate metastasis. However, little is known whether the endothelium would also influence the education of recruited monocytes. Here, we report that canonical Notch signalling through RBPJ in ECs is an important player in the education of TAMs and EOC progression. Deletion of *Rbpj* in the endothelium of adult mice reduced infiltration of monocyte-derived macrophages into the TME of EOC and prevented the acquisition of a typical TAM gene signature. This was associated with stronger cytotoxic activity of T cells and decreased tumour burden. Mechanistically, we identified CXCL2 as a novel Notch/RBPJ target gene. This angiocrine factor regulates the expression of CD44 on monocytes and subsequent cholesterol depletion of TAMs. Bioinformatic analysis of ovarian cancer patient data showed that increased CXCL2 expression is accompanied by higher expression of CD44 and TAM education. As such, EOC cells employ the tumour endothelium to secrete CXCL2 in order to facilitate an immunosuppressive microenvironment**.**

Introduction

High grade serous ovarian cancer is the deadliest type of all gynaecological cancers[1]. The high mortality rate is due to the fact that most women have already developed peritoneal metastasis at the time of diagnosis. Epithelial ovarian cancer (EOC) cells can directly infiltrate the peritoneal cavity to seed metastases, a process called transcoelomic metastasis[2]. Metastatic EOC cells initially reside in the omentum, where they undergo certain adaptations allowing them to spread throughout the whole peritoneal cavity.

Importantly, this peritoneal microenvironment is so immunosuppressive that even the infiltration of effector T cell does not *per se* correlate with better prognosis[3].

Peritoneal spread of tumour cells is accompanied by monocyte-derived macrophage (MN-derived macrophages) recruitment, which eventually become the most abundant myeloid cell type[4] and are a major contributor to the immunosuppressive TME in EOC[3]. Upon recruitment from blood to the tumour, monocytes differentiate into macrophages which are further educated by the TME. Eventually, tumour-associated macrophages (TAMs) strongly promote the progression of metastatic ovarian cancer[5]. However, little is known about the contribution of other stromal cells to the peritoneal spread of EOC cells and to macrophage education.

Monocytes must cross the vascular endothelial barrier before infiltrating peritoneal organs or the peritoneal fluid. Endothelial cells (ECs) not only form tubes for the transport of blood, but also produce soluble factors controlling the differentiation and function of adjacent cells. These angiocrine functions are highly context and organ specific[6,7]. In cancer, ECs provide angiocrine factors which influence tumour progression[8]. Therefore, we hypothesized that monocytes are influenced by ECs, for instance during transmigration, while infiltrating into peritoneal tissues.

Notably, tumours can alter the transcriptome of ECs[9,10] and this may also influence transmigrating monocytes. For example, endothelial Notch signalling activity is frequently higher in tumours like EOC and in the metastatic niche compared to ECs from non-tumourous tissue[11]. Notch signalling is a highly conserved cell-to-cell communication system. Ligand binding induces cleavage of the transmembrane Notch receptors releasing the intracellular domain (ICD) which enters the nucleus to alter gene transcription. This canonical signalling pathway relies on the DNA-binding protein RBPJ, which turns into a transcriptional activator upon binding of a Notch receptor ICD[12]. Sustained endothelial Notch1 signalling is associated with increased myeloid cell infiltration and metastasis[11]. The Notch pathway in ECs is a major regulator of angiogenesis, metabolism, angiocrine

functions and tumour cell transmigration[11,13-18]. Although EOC cells do not necessarily have to cross the endothelial barrier to spread throughout the peritoneum we hypothesized that endothelial Notch signalling could still influence EOC progression via transmigrating myeloid cells.

Here, we provide insights into the essential role of RBPJ in ECs for the recruitment of monocytes to the microenvironment of metastatic EOC and their proper education into pro-tumoural TAMs.

Results

Deletion of *Rbpj* in endothelial cells reduces EOC progression

Metastatic EOC cells seed initially in the omentum and later spread within the peritoneum. During these steps, tumour cells undergo transcriptional changes that allow them to further grow and colonise (**Fig. 1a**). The latter is strongly influenced by MN-derived macrophages[19]. To determine the contribution of canonical Notch signalling in ECs to myeloid cell infiltration and EOC progression, we used the tamoxifen-inducible VE-Cadherin (Cdh5) Cre^{ERT2} strain to delete *Rbpj* specifically in ECs of adult mice (*Rbpj*$^{i\Delta EC}$). This mouse model is well established and leads to robust gene recombination in ECs of several organs[14,15,17,18] (**Fig. 1b**). Under physiological conditions, there were no differences in blood vessel density in the larger omentum upon *Rbpj* deletion in ECs compared to controls (**Suppl. Fig. 1a,b**). However, upon intraperitoneal injection of ID8 cells mimicking metastatic EOC, the omenta showed evidence of tumour nodule growth (**Fig. 1c**) and had significantly higher vessel density in *Rbpj*$^{i\Delta EC}$ mice compared to control animals (**Fig. 1d**). The density of endothelial coverage with α-smooth muscle actin-positive mural cells was, however, unchanged (**Suppl. Fig. 1c**). Despite increased vessel density, tumour burden in omenta of *Rbpj*$^{i\Delta EC}$ mice was significantly lower than that in their littermate controls (**Fig. 1e**). Moreover,

peritoneal spread of tumour cells was significantly reduced as well in *Rbpj*$^{i\Delta EC}$ mice (**Fig. 1f**) concluding that deletion of *Rbpj* in ECs reduces EOC progression and metastasis.

Deletion of endothelial *Rbpj* decreases monocyte-derived macrophage recruitment

Next, we analysed the immune cell compartment of our EOC model since it is a major contributor to tumour progression. High Notch signalling activity in ECs induces VCAM1 expression, which promotes leukocyte extravasation[11,20]. However, VCAM1 expression was unchanged between *Rbpj*$^{i\Delta EC}$ and their controls littermates (**Suppl. Fig. 2a**). Nevertheless, whole-mount staining of omenta revealed that there was a reduction in immune cells inside tumour nodules of *Rbpj*$^{i\Delta EC}$ mice compared to controls (**Fig. 2a** and **Suppl. Fig. 2b**). Interestingly, tumours in control mice contained more cells with a large vacuolated cytoplasm, reminiscent of macrophages. Therefore, we analysed this cell population in greater detail. Tumour-bearing omenta from *Rbpj*$^{i\Delta EC}$ mice contained less CD11b^{+} cells within tumour nodules, although this reduction was not statistically significant (**Fig. 2b**). In order to better determine the macrophage subpopulations responsible for the observed decrease in CD11b^{+} cells; we studied the myeloid and macrophage populations in the peritoneal cavity to understand whether RBPJ in ECs could play a role in their composition. After four weeks of tumour growth, there were no significant differences in the total amount of myeloid cells or macrophages (**Fig. 2c,d**). However, we found decreased numbers of small peritoneal macrophages (SPMs), which are MN-derived macrophages characterized as MHC-II^{hi}/F4/80^{low} (**Fig. 2e**) and CCR2^{+}/Tim4^{-} (**Fig. 2f**). Notably, in naïve (tumour-free) conditions, endothelial *Rbpj* deletion had no effect on peritoneal macrophage populations (**Suppl. Fig. 2c-f**). These data suggest that the tumour-driven recruitment of monocytes into the peritoneum is impaired upon endothelial deletion of *Rbpj*.

To further dissect endothelial chemotaxis in a more simplified *in vitro* system, we switched to the human system and measured transmigration of human CD14^{+} monocytes

through a monolayer of human ECs in a transwell insert. Chemotaxis was stimulated by SK-OV-3 human ovarian cancer cells below the insert (**Fig. 2g**). *RBPJ* deletion in human umbilical vein ECs (HUVECs) resulted in significantly decreased monocyte transmigration rates compared to control HUVECs (**Fig. 2h**). This further suggests that canonical Notch signalling in ECs is important to facilitate monocyte recruitment into the TME.

Canonical Notch signalling in ECs regulates monocyte recruitment through CXCL2

We have previously analysed the transcriptional induction of chemokines in HUVECs upon Notch1 ICD (N1ICD) overexpression[11]. Based on this, we transduced *RBPJ*-deficient HUVEC and control cells with N1ICD to determine which of those transcriptional changes require *RBPJ*. The chemokines that were induced by N1ICD through RBPJ were *CCL1, CCL21, CXCL12,* and *CXCL2* (**Fig. 3a**) and we excluded those that were not induced through RBPJ (**Suppl. Fig. 3a-b**). Next, we measured the mRNA expression levels of these chemokines in peritoneal adipose tissue obtained from *Rbpj*$^{i\Delta EC}$ mice. This revealed that there was lower *Cxcl2* expression in peritoneal adipose tissue from *Rbpj*$^{i\Delta EC}$ mice compared to littermate controls, whereas the other chemokines analysed were not changed (**Fig. 3b**). Analysis of the same cytokines in endothelial-specific N1ICD mice[11,15], exposed that higher endothelial Notch1 signalling activity led to higher *Cxcl2* expression in peritoneal adipose tissue (**Fig. 3c**).

In silico analysis showed that the mouse and human *Cxcl2* gene contains RBPJ-binding sites in the promoter region (**Fig. 3d**). Consistently, cultured human ECs secreted higher CXCL2 protein levels after being transduced with N1ICD expressing adenovirus compared to GFP-transduced control cells (**Fig. 3e**).

These data revealed that canonical Notch signalling induces CXCL2 expression in ECs. CXCL2 is known to attract granulocytes but also to a lesser extend monocytes[21]. As such, it poses as an interesting endothelial Notch target, which could mediate the observed

effects on monocyte recruitment into the TME. To evaluate whether CXCL2 was capable of attracting monocytes, we performed transwell chemotaxis experiments and observed that recombinant CXCL2 induced monocyte chemotaxis (**Fig. 3f**). Next, we silenced *CXCL2* expression in ECs using shRNA, which led to an about 50% reduction of CXCL2 protein expression (**Fig. 3g**). Compared to non-silencing control, this reduction of CXCL2 levels was already capable of reducing the numbers of monocytes transmigrating through ECs towards SK-OV-3 cells (**Fig. 3h**). In summary, the data implicate that the endothelial RBPJ/CXCL2 axis contributes to monocyte recruitment into the peritoneum during transcoelomic metastasis.

***Rbpj* in ECs is necessary for tumour-mediated TAM education**

Recruited monocytes differentiate into macrophages which are further educated by tumour cells to become tumour-promoting macrophages. Macrophage education in EOC is facilitated by hypersensitivity towards IL4, which is induced by tumour cell-mediated cholesterol depletion[4]. We sought to understand whether lack of *Rbpj* in ECs could influence macrophage phenotypes. To assess this, we isolated newly recruited MN-derived macrophages ($CD11b^+/F4/80^+/CCR2^+$) (**Fig. 4a**) and obtained their transcriptomic profile by microarray analysis. Gene set enrichment analysis (GSEA) comparing MN-derived macrophages from $Rbpj^{i\Delta EC}$ and control tumour-bearing mice revealed that *Rbpj* in ECs is necessary to acquire the typical phenotype of TAM in this model of metastatic EOC (**Fig. 4b**). As such, tumour cells could not fully educate MN-derived macrophages in mice lacking endothelial *Rbpj.*

Transcriptomic profiling via Ingenuity Pathway Analysis (IPA) determined that IL4 was the most downregulated signalling pathway in MN-derived macrophages obtained from $Rbpj^{i\Delta EC}$ tumour bearing mice (**Fig. 4c**). IPA and pathway analysis showed that genes important for cholesterol synthesis were downregulated in MN-derived macrophages from $Rbpj^{i\Delta EC}$ mice (**Fig. 4d,e**). We then employed a cholesterol homeostasis gene set from TAMs

obtained 21 days after tumour injection[4], representing EOC-induced cholesterol metabolism in TAMs. GSEA showed that this gene set was significantly enriched in newly recruited macrophages coming from control tumour-bearing mice (**Fig. 4f**), indicating that *Rbpj* in ECs is necessary for cholesterol depletion in TAMs.

Cholesterol depletion is mediated by tumour cell-secreted high molecular weight hyaluronan (HMW-HA). The interaction with HA receptors, such as CD44, in macrophages leads to cholesterol efflux through ABC transporters[4]. In order to understand whether *Rbpj* in ECs could be important for CD44 expression in monocytes, we co-cultured human monocytes with HUVECs lacking *RBPJ* or with respective controls. Monocytes co-cultured with *RBPJ*-deficient HUVECs, had less CD44 on their membrane than those incubated with control HUVECs (**Fig. 4g**). Next, when incubating bone marrow-derived macrophages (BMDMs) with conditioned medium (CM) from immortalized mouse cardiac endothelial cells (MCECs) lacking *Rbpj* (CRISPR-Cas9 mediated), macrophages expressed less *Cd44* (**Fig. 4h**) and *Mmp9* (**Fig. 4i**), a known CD44 target gene. This indicates that a secreted angiocrine factor regulated by the transcription factor RBPJ in ECs is necessary for the regulation of CD44 in macrophages. To understand whether this would also happen *in vivo*, *Rbpj*$^{i\Delta EC}$ and control mice were injected with thioglycolate to induce MN-derived macrophage recruitment in the absence of tumour cells. We found that MN-derived macrophages in *Rbpj*$^{i\Delta EC}$ mice expressed significantly less *Cd44* than those in control mice (**Fig. 4j**), confirming that RBPJ in EC is essential for *Cd44* regulation in MN-derived macrophages *in vivo*.

Considering the important role that CXCL2 had in monocyte recruitment in *Rbpj*$^{i\Delta EC}$ tumour bearing mice and that higher level of CXCL2 in serum is associated not only with myeloid cell infiltration into the TME, but also with worse prognosis for EOC patients[22], we decided to analyse its role in regulating CD44 expression. Indeed, when stimulating BMDMs with CXCL2, *Cd44* expression was increased (**Fig. 4k**). Moreover, since CD44 is a membrane-bound receptor, we analysed by immunofluorescence whether also its cellular localization could be altered. We observed that CXCL2 stimulation of BMDMs increased the

presence of CD44 on the plasma membrane, which would consequently increase its accessibility to hyaluronic acid (**Fig. 4l** and **Suppl. Fig. 4**).

The TAM gene signature is enriched in human ovarian carcinoma samples with high CXCL2 expression

The data presented so far indicate that the angiocrine factor CXCL2, which is under transcriptional control of Notch/RBPJ signalling, preconditions monocytes to be educated by tumour cells in the TME. In order to evaluate the relevance of this, we analysed *CXCL2* and *CD44* mRNA expression levels in publicly available data sets from the Cancer Genome Atlas (TCGA). Remarkably, the stratification of ovarian cancer patients in 25% upper ($CXCL2^{hi}$) and lower ($CXCL2^{low}$) *CXCL2* expression showed that $CXCL2^{hi}$ patients displayed significantly more expression of *CD44* (**Fig. 5a**). These data suggest a positive correlation between *CXCL2* and *CD44* expression in human tumours. Our data indicate that CXCL2-mediated CD44 induction reflects the ability of tumour cells to educate TAMs. Therefore, the correlation in expression between CXCL2 and CD44 should in turn have implications on TAM education. Therefore, we performed GSEA comparing $CXCL2^{hi}$ and $CXCL2^{low}$ patients using the abovementioned TAM signature. We observed that the TAM signature was significantly enriched in $CXCL2^{hi}$ patients (**Fig. 5b**), indicating that the increased CD44 expression in these patients consequently impacts TAM education.

When analysing difference between $CXCL2^{hi}$ and $CXCL2^{low}$ patients, we found an expected upregulation of chemotactic response and myeloid cell recruitment, as shown by gene ontology (GO) term analysis in $CXCL2^{hi}$ patients (**Suppl. Fig. 5**), supporting the role of CXCL2 in controlling the myeloid cell compartment of tumours. Interestingly, we again identified cholesterol metabolism as one of the most downregulated pathways in $CXCL2^{low}$ patients (**Fig. 5c**). Instead, $CXCL2^{hi}$ patients showed induction of pathways such as lipid and atherosclerosis, thus suggesting opposite profiles (**Fig. 5d**). Indeed, GSEA showed that the

same cholesterol metabolism gene set previously employed was significantly enriched in CXCL2^{hi} cohort (**Fig. 5e**), indicating a similar cholesterol depletion as the one occurring in peritoneal macrophages of our mouse model.

TAM education mediated by endothelial *Rbpj* affects T cell cytotoxicity

One of the genes downregulated in MN-derived macrophages from *Rbpj*$^{i\Delta EC}$ tumour-bearing mice is *Cd74* (**Fig. 4b**). CXCL2 is a ligand for CXCR2[21], and CD44 is part of a receptor complex that contains CD74 and CXCR2[23,24]. Moreover, CD44 plays an important role in CD74-mediated signal transduction[25]. *In silico* analysis showed that CD74 interacts closely with CD44 and CXCR2 (**Fig. 6a**). Besides, CD74 has been reported to be important in TAMs in brain metastasis[26], and CD74 expression has been associated with worse prognosis in metastatic ovarian cancer[27]. Furthermore, CD74 was associated with an immunosuppressive phenotype in macrophages[28]. We decided to investigate whether the downregulation of CD74 could have a consequence on TAM behaviour. For that, we analysed publicly available data sets where IL4 responses in CD74-deficient macrophages were analysed[29]. GSEA showed that TAM signature was enriched in wild-type macrophages, indicating that CD74 is not only regulated by IL4, but also necessary for TAM education (**Fig. 6b**). We extracted a signature with the 500 most enriched genes in control compared to CD74-deficient macrophages stimulated with IL4 (CD74-mediated signature), representing a group of genes induced by IL4 through CD74 activation. When comparing newly recruited MN-derived macrophages from our EOC model by GSEA, we found that the CD74-mediated signature was significantly enriched in macrophages isolated from control mice compared to *Rbpj*$^{i\Delta EC}$. This suggests that newly recruited macrophages from *Rbpj*$^{i\Delta EC}$ mice cannot induce their immunosuppressive phenotype due to downregulation of CD74-mediated genes (**Fig. 6c**).

To verify the specific effect on the newly recruited macrophages, we repeated the same analysis on resident macrophages ($CD11b^+/F4/80^+/CCR2^-$), in which *Cd74* is not differentially expressed between $Rbpj^{i\Delta EC}$ tumour-bearing and control mice, and found no enrichment of this gene set in any group, confirming that *Rbpj* deletion in ECs only affects *Cd74* expression in newly recruited MN-derived macrophages (**Suppl. Fig. 6**). In summary, only macrophages that have crossed the EC barrier as monocytes were affected by the lack of *Rbpj* in the endothelium.

It has been previously reported that TME in metastatic ovarian cancer is highly immunosuppressive and infiltration with immune effector cells has little impact in patients' outcome[3]. This immunosuppressive microenvironment has been attributed to TAMs[3]. For this reason, we wanted to test whether impaired TAM education could impact on the phenotype of the TME. We isolated T cells from tumour-bearing $Rbpj^{i\Delta EC}$ mice and their littermate controls six weeks after intraperitoneal injection of ID8 cells (**Fig. 6d**). Results demonstrated that T cells derived from $Rbpj^{i\Delta EC}$ mice were more efficient in killing cultured ID8 cells (**Fig. 6e**). This confirms that impairment in TAM education has a direct impact on T cell cytotoxicity. In addition, the analysis of T cell populations in peritoneal cavity from tumour-bearing mice revealed that, although the total frequency of T cells was not changed, the cytotoxic $CD8^+$ T cell population was significantly increased in $Rbpj^{i\Delta EC}$ mice compared to their littermate controls (**Fig. 6f**). In summary, our data reveal that *Rbpj* in ECs is necessary for tumour cell-mediated education of MN-derived macrophages into TAMs (**Fig. 6g**).

Discussion

Collectively, this study provides evidence about a novel angiocrine axis influencing the tumour immune microenvironment. We show how Notch/RBPJ-mediated transcription in ECs, which is frequently hyperactive in tumours[11], is required for CXCL2-mediated monocyte

chemotaxis, induction of CD44 expression on monocytes, and the adoption of a TAM gene signature in metastatic ovarian cancer.

Mice with EC-restricted *Rbpj loss* had impaired ovarian carcinoma growth in the omentum and peritoneum and lower numbers of MN-derived macrophages in the peritoneal fluid. These macrophages are essential for metastatic ovarian cancer development[4,30]. As such, the endothelium can influence tumour progression and metastasis by altering the immune status of the TME. Specifically, we observed that monocyte recruitment is potentiated, at least in part, through the release of *Rbpj*-mediated CXCL2 from ECs. Interestingly, higher serum levels of CXCL2 in ovarian cancer patients are associated with myeloid cell infiltration, poor prognosis and chemoresistance[31]. It should be noted that this chemokine has been traditionally associated with the recruitment of neutrophils[21]. However, there is evidence that CXCL2 also plays a role in the regulation of TAMs, especially those derived from monocytes. For instance, the CXCL2 receptor CXCR2 on monocytes and macrophages is important for the education of TAMs in prostate cancer[32].

CXCR2 blockade has also been shown to re-sensitize ovarian cancer to cisplatin treatment[33]. Here we suggest that the CXCL2/CXCR2 axis might also have a role in the recruitment and education of macrophages in ovarian cancer. By separating newly recruited macrophages from macrophages that have reside in the peritoneal cavity for a longer period, we observed that endothelial RBPJ is necessary for the education into TAMs by tumour cells. Specifically, we report that MN-derived macrophages in contact with ECs lacking RBPJ had a lower expression of the HA receptor CD44. This receptor gets stimulated by HMW-HA produced by tumour cells to induce cholesterol depletion in macrophages, a crucial mechanism by which tumour cells educate TAMs[4]. Therefore, we propose that through this mechanism ECs can pre-condition MN-derived macrophages and contribute to their immunosuppressive phenotype within the tumour microenvironment. Indeed, the data showed that important genes involved in cholesterol depletion were reduced in MN-derived macrophages from mice lacking RBPJ in their ECs. Consistently, T cells isolated from this

TME were more efficient at killing tumour cells, confirming the reduced immunosuppressive potential of the MN-derived macrophages.

In conclusion, we demonstrate that peritoneal ECs are critically involved in the recruitment and education of MN-derived macrophages in ovarian carcinoma.

Material and methods

Animal models

All animal procedures were approved by the local institutional animal care and use committee (RP Karlsruhe, Germany and DKFZ) and performed according to the guidelines of the local institution and the local government. Female C57BL/6 mice were group-housed under specific pathogen-free barrier conditions.

Administration of tamoxifen diluted in sterile peanut (P2144, Sigma-Aldrich, St. Louis, USA) in 8 to 12-week-old randomized mice was performed by oral gavage once with 100 µl (1 mg tamoxifen)[34]. Control mice, which did not express Cre^{ERT2} were also treated with tamoxifen.

Model of ovarian cancer: Three weeks after gene recombination, $5x10^6$ ID8-luciferase (ID8-luc) ovarian cancer cells were administered i.p. in PBS. For peritoneal lavage after sacrificing the mice, 5 ml of ice-cold PBS (Gibco/Thermo Fisher Scientific, NY, USA) was injected i.p., and after a careful massage to mobilize cells, peritoneal fluid was collected. For analysis of ID8-luc tumour growth the cell suspension was centrifuged and supernatant was collected. The cell pellet was suspended in 1 mL PBS and 100 µL were used to determine the luciferase activity. 100 µL cell suspension were centrifuged and the cell pellet was suspended in 100 µL lysis buffer (Promega) and 20 µL of lysed cells were pipetted into white 96-well plate in triplicates. 50 µL of LAR substrate (Promega) was added to the lysed cell suspension and luminescence signal was determined using the plate reader (ClarioStar,

BMG Labtech). For analysis of immune cell recruitment into the peritoneal cavity the collected peritoneal cell suspension was centrifuged and red blood cells in the cell pellet were lysed with 1 mL ACK (Thermo Fisher Scientifics). After washing the cell suspension was counted using Neubauer Counting chamber and $1x10^6$ cells were used for flow cytometry staining.

Model of peritoneal inflammation: To obtain newly recruited peritoneal macrophages, 1 mL thioglycolate (2 mg/mL in H_2O; B2551, Sigma-Aldrich) was injected into the peritoneum three weeks after gene recombination. MN-derived macrophages were isolated 24 hours after thioglycolate injection by their adherence to non-treated plastic petri dishes. Briefly, after incubation of single cells in a petri dish for 30 min at 37C, non-adherent cells washed away with PBS.

Flow cytometry

For flow cytometry analysis, cells were suspended in 1 mL PBS with 2% FCS (Biochrom). Cell suspension was incubated with the different fluorophore-coupled primary antibodies for 20 min on ice. The following antibodies were used: CD45 (552848), CD11b (552850) and CD4 (560468) and CD8 (557654) from BD Biosciences (Bedford, MA, USA); CD3 (100203), F4/80 (123128), CCR2 (150608), CD44 (mouse and human 103007), CD74 (mouse (151005) and human (326811)) from BioLegend (St. Diego, CA, USA), MHCII (47-5321-80, Life Technologies/Thermo Fisher Scientific, NY, USA) and Tim4 (12-5866-82, Life Technologies/Thermo Fisher Scientific, NY, USA). Concentration of the different antibodies was determined by titration. In the meanwhile, compensation beads (UltraComp eBeads, Thermo Fisher) of the used primary antibodies were prepared. After staining, cells were washed with PBS and stored on ice until acquisition. Acquisition was performed using BD FACSCanto TM II, BD LSR for analysis or Aria for cell sorting (BD Biosciences).

Experiments were analysed using FlowJo Software. Flow cytometer results in percentage were extrapolated to the total number of cells obtained from the cell counting.

Whole mount staining

The omentum was fixed for 1 hour in 1% PFA at room temperature and washed with PBS. Tissues were washed three times for 5 min with permeabilization buffer (PBS, 0.1% BSA and 0.2% Triton X-100) and treated with 0.5 mL blocking buffer (5% donkey serum diluted PBS-T) for 1 hour at room temperature. Primary antibodies, CD45 (BD 553076) and luciferase (ab185924), were diluted in PBS-T with 2% donkey serum. Next day, samples were washed three times with PBS- 0.3% Tween. Afterwards secondary antibodies (1:200) were incubated for 1 hour at room temperature, washed three times with PBS 0.3% Tween and incubated with DAPI (1:10.000) for 15 min. Next, samples were incubated with clearing solution (FUnGi: 60% glycerol (vol/vol), 2.5M fructose, 2.5M urea, 10mM Tris Base, 1.0mM EDTA) at 4 °C overnight. Coverslips were mounted with FUnGi clearing solution and imaged with a confocal microscope (LSM 710, Carl Zeiss). All images were processed with ZENblue software (Carl Zeiss, Germany). Average mean intensities per image were counted with ImageJ software (NIH, Bethesda, MD, USA).

Immunohistochemistry

Paraffin-embedded sections (3 µm) were de-paraffinized and re-hydrated in xylene and step-wise reductions in alcohol concentrations. H&E staining was performed according to standard protocols. Cytokeratin DAB and CD11b: antigen retrieval was performed at pH9 with citrate buffer. Primary antibodies CD11b (abcam, ab133357, 1:200), and Pan-cytokeratin (undiluted, ZUC001-125), diluted in blocking solution, were incubated at 4°C overnight. After washing, sections were incubated with secondary antibodies coupled with ZytoChem Plus (HRP) Polymer anti-mouse, (ZYTOMED, ZYT-ZUC050-006) and ZytoChem

Plus (AP) Polymer anti-rabbit, (ZYTOMED, ZYT-ZUC031-006) diluted in antibody diluent (Cell Signaling) for one hour at room temperature. Afterwards, slides were treated with DAB Substrat Chromogen, Zytomed, ZYT-DAB057 and AP Red Kit, Zytomed, ZUC001-125. Immunofluorescence staining: primary antibodies: CD31 (Abcam, ab28364, 1:50), VCAM (Vcam, ab134047, 1:200) and αSMA (Sigma-Aldrich, A5228, 1:200) were diluted in blocking solution. Fluorophore-conjugated secondary antibodies (Thermo Fisher Scientific) were diluted in antibody diluent (Cell Signaling) together with isolectin-B4 (Thermo Fisher Scientific, I32450). Images were obtained with slide scanner (Zeiss Axio Sacn.Z1, Carl Zeiss) and a confocal microscope (LSM 710, Carl Zeiss). All images were processed with ZENblue software (Carl Zeiss, Germany). Image quantification were proceeded with ImageJ software (NIH, Bethesda, MD, USA).

Cell culture

Murine cardiac ECs (MCEC) were purchased from tebu-bio and cultured on gelatin-coated surfaces in in DMEM containing 1 g/L D-glucose, 5 % FCS, 5 % HEPES, 100 units/ml penicillin and 100 µg/ml streptomycin.

HUVEC were grown and maintained until passage 5 in Endopan-3 Growth Medium containing 3% FCS and supplements (Pan-Biotech).

SK-OV-3 cells were kindly donated by Dr. Christiane Opitz (DKFZ, Heidelberg) and cultured in DMEM containing 1 g/L D-glucose, 10 % FCS, 5 % HEPES, 100 units/ml penicillin and 100 µg/ml streptomycin.

ID8-luc cells were kindly donated by provided by Prof. Frances Balkwill (Barts Cancer Institute, London, UK) and cultured in DMEM containing 1 g/L D-glucose, 10 % FCS, 5 % HEPES, 100 units/ml penicillin and 100 µg/ml streptomycin.

All cell culture experiments were performed in a laminar flow hood and cells cultured at 37°C and 95% relative humidity and 5% CO_2. Cell culture were tested on a regularly basis for mycoplasma contamination periodically and before injecting the tumour cells into the mice.

To study the role of RBPJ in the regulation of Notch target genes, human umbilical vein endothelial cells (HUVECs) were infected with lentivirus constructs for CRISPR/Cas9 (Addgene plasmid #52961, lentiCRISPR v2) induced knock-out for *Rbpj*[35] . After 48 hours, cells were infected with adenovirus (LifeTechnologies; pAD/CMV-V5-DEST) overexpressing GFP as control or N1ICD.

Isolation of peripheral blood nuclear cells (PBMC) from buffy coats

Human buffy coats were purchased from blood donation service DRK Mannheim, Germany. Peripheral blood nuclear cells (PBMC) were isolated by gradient centrifugation using Biocoll density solution (L6715; Biochrom). Human buffy coat was diluted 1:1 with PBS and added to the Biocoll density solution. This mixture was centrifuged at 430g for 20 min at room temperature. After centrifugation, the white intermediate phase containing leukocytes was collected and washed with PBS. To perform a positive isolation of monocytes, CD14 MACS beads were used with the LS column (130-042-402; Milentyi Biotec). The isolation of $CD14^+$ monocytes was performed following the manufacture's protocol.

Transwell assay

Human ovarian cancer cells were seeded at 100,000 cells/ml in 500 µl RPMI medium without FCS for 48 hours. For the ECs monolayer, inserts were coated for 2 hours with 2 µg/ml fibronectin (1918-FN-02M; R&D Systems) in PBS. 50,000 human ECs (*RBPJ* knock-out or shRNA for *CXCL2* (pLKO.1; Sigma Aldrich) and respective controls) were seeded on

top of the insert membrane for 48 hours. To analyse monocyte transmigration, 200,000 $CD14^+$ cells were stained with carboxyfluorescein succinimidyl ester (CSFE; ThermoFischer) and added onto the endothelial monolayer. The transwell plate was incubated for 2 hours. For the chemotaxis assay with the recombinant proteins, transmigration of 50,000 $CD14^+$ cells were analysed towards 60 ng/mL CXCL2 (PeproTech GmbH) in RPMI medium without FCS for 30 min. After incubation, the remaining cell suspension in the upper well was aspirated and the transwell was cleaned with a cotton swab. The migrated cells were fixed with 4% PFA for 20 min at room temperature. Imaging of transwell was performed with Cell Observer (Carl Zeiss). From each transwell five evenly spaced field picture were taken using 20x objective and analysis was performed with Image J software.

Enzyme-linked Immunosorbent Assay (ELISA)

Protein expression of CXCL2 (MIP-2) was quantified using an enzyme-linked immunosorbent assay (ELISA; Abcam ab184862). Cell culture supernatant was collected after 24 hours and ELISA was performed following the manufacture's protocol.

Bone marrow-derived macrophages (BMDMs) differentiation

Mouse macrophages were derived from the bone marrow of wild-type C57BL/6 mice. Femurs and tibiae were flushed several times with DMEM and collected cells were centrifuged. Bone marrow cells were suspended in media and seeded on 10 cm petri dishes (Corning). To differentiate these cells into macrophages, 10 ng/ml M-CSF (PeproTech GmbH) were added to Dulbecco's modified Eagle's medium (DMEM) (Thermo Fisher) supplemented with 10% fetal calf serum (FCS) (Biochrom, UK). Differentiation occurred within seven days. Cells were afterwards stimulated with indicated amount of recombinant protein CXCL2 (250-15-20, PeproTech GmbH) in DMEM medium without FCS or conditioned medium of endothelial cells.

Immunostaining

BMDMs were cultured in DMEM with 10% FCS (Biochrom, UK) and 250,000 cells/well were seeded into 24-well plates on top of coverslips. BMDMs were treated with 40 ng/mL CXCL2 (PeproTech GmbH) in DMEM without FCS for 72 hours. Cells were washed with PBS and fixed with 4% PFA for 10 min. Then, the coverslips were washed three times for 5 minutes with PBS, permeabilized with PBS with 0.1 % Triton X-100 for 10 minutes and blocked for 30 min in blocking buffer (PBS in 5% FCS with 0.1% Tween 20 and 100 mM glycine) for 1 hour at room temperature. The coverslips were incubated with antibody against CD44 (1:1000) (Abcam, ab124515) and CD45 (1:500) (BD 553076) overnight at 4°C. The coverslips were rinsed three times with blocking buffer and incubated with a secondary antibody coupled to Alexa Fluor-488 and Alexa Fluor-546 (1:200) for 1 hour. The coverslips were washed and incubated with a DAPI solution before they were washed again. Coverslips were mounted and imaged with a confocal microscope (LSM 710, Carl Zeiss). All images were processed with ZENblack software (Carl Zeiss, Germany).

cDNA synthesis and qPCR

RNA isolation from cell culture was performed using the InnuPrep Mini Kit (Analytik Jena) according manufacture's protocol. RNA isolation form tissue was performed using PicoPure RNA Isolation Kit (Acturus, Life Technology). 1 mL Trizol was added to the tissue and homogenized for 1 min and a frequency of 30/sec. After disruption of the tissue, 200 µL chloroform were added and mixed by inverting several times followed by a centrifugation step for 15 minutes 12.000g at 4°C. Further RNA isolation steps were performed using the manufacture's protocol. RNA concentration was measured using a Nanodrop 100 (Thermo Fisher Scientific). Reverse transcription of isolated RNA into complementary DNA was performed using High-Capacity cDNA Reverse Transcription Kit (Thermo Fisher Scientific).

Quantitative real-time PCR (qPCR) was performed with SYBR Green PCR mix (Applied Biosystems) on a QuantStudio3 Real-time PCR system (Applied Biosystems). Resulting fold changes were calculated using the $2^{\Delta\Delta CT}$ method and mRNA expression was normalized to the housekeeping gene (*Cph* for murine and *HPRT* for human samples).

Primers used for mouse genes

Gene Name	Forward Primer	Reverse Primer
Cph	ATGGTCAACCCCACCGTG	TTCTTGCTGTCTTTGGAACTTTGTC
Ccl1	CTGCTGCTTGAACACCTTGA	GGTGATTTTGAACCCACGTT
Ccl21	ACCCAAGGCAGTGATGGA	CAGGGTTTGCACATAGCTCA
Cxcl2	CCAACCACCAGGCTACAGG	GCGTCACACTCAAGCTCTG
Cxcl12	GTCCTCTTGCTGTCCAGCTC	TAATTTCGGGTCAATGCACA
Cd44	TCGATTTGAATGTAACCTGCCG	CAGTCCGGGAGATACTGTAGC
Mmp9	CTGGACAGCCAGACACTAAAG	CTCGCGGCAAGTCTTCAGAG

Primers used for human genes

Gene Name	Forward Primer	Reverse Primer
HPRT	TGTTGTAGGATATGCCCTTGACT	CTAAGCAGARGGCCACAGAAC
CCL1	CATTTGCGGAGCAAGAGATT	TGCCTCAGCATTTTTCTGTG
CCL2	CAGCCAGATGCAATCAATGCC	TGGAATCCTGAACCCACTTCT
CCL21	CCCAGCTATCCTGTTCTTGC	TCAGTCCTCTTGCAGCCTTT
CXCL2	GGCAGAAAGCTTGTCTCAACCC	CTCCTTCAGGAACAGCCACCAA
CXCL5	AGCTGCGTTGCGTTTGTTTAC	TGGCGAACACTTGCAGATTAC
CXCL8	AAGAAACCACCGGAAGGAAC	AAATTTGGGGTGGAAAGGTT
CXCL12	ATTCTCAACACTCCAAACTGTGC	ACTTTAGCTTCGGGTCAATGC

Cytotoxicity assay

To analyse the T cell killing potential by the lactate dehydrogenase (LDH)-Cytotoxicity Assay Kit (Ab65393, Abcam), ID8 cells (7,500 ID8 cells in 100 µL DMEM medium) were seeded in a 96-well plate one day before T cell sorting. T cells were sorted from tumour bearing *Rbpj*$^{i\Delta EC}$ and control mice after six weeks of tumour growth and 10,000 $CD3^+$ cells were co-cultured with ID8 cells in technical triplicates including untreated control and blank. After overnight incubation, cytotoxicity and killing potential was measured by LDH amount in the cell supernatant using the LDH-Cytotoxicity Assay Kit (Ab65393, Abcam) following the manufacturer's protocol.

In silco analysis of promotor region

To determine RBPJ binding sites[36] (5´-GTGGGAA-3´) in the promotor region of the murine (NM_009140; chr5+:90902580-90903927) and human (NM_002089; chr4-:74100502-74099123) CXCL2-encoding gene, we used ApE plasmid Editor by M. Wayne Davis (https://jorgensen.biology.utah.edu/wayned/ape/).

In silico protein-protein interaction

We used the Search Tool of Interacting Genes/Proteins database (STRING v11.5) to perform *in silico* protein-protein interaction analysis[37]. Given CXCR2 protein as input, STRING can search for their neighbour interactors, the proteins that have direct interactions with the inputted proteins; then STRING can generate the PPI network consisting of all these proteins and all the interactions between them. All the interactions between them were derived from high-throughput lab experiments and previous knowledge in curated databases at medium level of confidence (score ≥ 0.40).

Gene set enrichment analysis (GSEA)

GSEA (Broad Institute) was used to determine if a list of genes (gene signature) was enriched between different groups. A defined list of genes exhibits a statistically significant bias in their distribution (false discovery rate (FDR)) within a ranked gene list using the software GSEA[38] resulting to an enrichment in one of the compared groups (normalized enrichment score (NES)) obtained from microarray or public available data sets as indicated in the figure legend.

Ingenuity Pathway Analysis (IPA)

IPA software (Qiagen) was used to identify predicated upstream regulators and differentially regulated pathways in newly recruited macrophages (based on microarray data). For the analysis of data, fold-changes were uploaded to the software. Differentially regulated pathways and upstream regulator analysis was performed from obtained microarray data.

Pathway analysis

Pathway analysis were obtained from public external databases (EnrichR) and analysed as -2log fold changes.

Human ovarian cancer patient RNAseq data analysis

Human ovarian cancer patient bulk tumour RNA-sequencing data was obtained from the Cancer Genome Atlas (TCGA) database. Stratification in $CXCL2^{high}$ and $CXCL2^{low}$ patients was performed using R Studio software. Patients were assigned to the different groups using *CXCL2* expression below the first or higher than the third quartile. Normalised raw counts of CD44 were plotted comparing the two different groups.

Statistical analysis

Normality was tested when sample size allowed it. Those samples with normal distribution where compared using Students´ t-test (with Welch's correction when groups had different sizes). When normality was rejected, Mann-Whitney U-test was used. Comparison analysis was performed with analysis of variance (ANOVA) with Tukey post-test when more than two groups were analysed. Statistical analysis and the generation of the graphs were performed using GraphPad Prism 9 (GraphPad Software, Inc.; La Jolla, CA, USA).

Schematic Figures

Schematics were created using BioRender.com.

Acknowledgements

We thank Ralf Adams (MPI Münster, Germany) for providing Cdh5-CreERT2 mice, we kindly acknowledge Dr. Christiane Opitz for providing the SK-OV-3 cell line and Frances Balkwill (Barts Cancer Institute, London, UK) for providing ID8-luc cells. We thank the Light Microscopy core facility, the Microarray Unit, the Flow Cytometry core facility and animal caretakers of the German Cancer Research Center (DKFZ) for providing excellent services. We would like to thank Damir Krunic (DKFZ, Light Microscopy Core Facility) in particular for his help with FIJI software data analysis.

This work was funded by the Deutsche Forschungsgemeinschaft (DFG) project 394046768 - SFB1366 projects C4, C2 (to A.F.& A.C.), SPP 1937 (CE 140/2-2 to A.C.), TRR179 (TP07 to A.C.), SFB-TRR156 (B10N to A.C.); the Cooperation Program in Cancer Research of the German Research Cancer Center (DKFZ) and the Israeli Ministry of Science and Technology (MOST) (to A.F.), DFG project 419966437, Deutsche Krebshilfe project 70113888, Ministerio de Ciencia e Innovación (PID2020-115048RB-I00) (to J.R-V.). The Science Ministry of Spain or the Health Ministry (ISCIII) receives support from the EU and its ERDF program. Part of the equipment used in this work has been funded by Generalitat Valenciana and co-financed with ERDF funds (OP ERDF of Comunitat Valenciana 2014-2020).

Author Contributions

R.M., E.A-S, I.M., S.B., L.W., L.J., T.Z., J.T., F.A.R., A.S., B.D.G., J.R-V. performed experiments. A.C., T.B., A.F. and J.R-V. contributed to analysis of results. A.F. and J.R-V. conceived the original hypothesis. R.M., E.A-S., A.F. and J.R-V. planned experiments. R.M., E.A-S., J.R-V. and A.F. wrote the manuscript. J.R-V. directed and supervised the work.

Competing Interests statement

Authors declare that they have no competing interests.

References

1 Ferlay, J. *et al.* Cancer statistics for the year 2020: An overview. *Int J Cancer*, doi:10.1002/ijc.33588 (2021).

2 Kipps, E., Tan, D. S. & Kaye, S. B. Meeting the challenge of ascites in ovarian cancer: new avenues for therapy and research. *Nat Rev Cancer* **13**, 273-282, doi:10.1038/nrc3432 (2013).

3 Hensler, M. *et al.* M2-like macrophages dictate clinically relevant immunosuppression in metastatic ovarian cancer. *J Immunother Cancer* **8**, doi:10.1136/jitc-2020-000979 (2020).

4 Goossens, P. *et al.* Membrane Cholesterol Efflux Drives Tumor-Associated Macrophage Reprogramming and Tumor Progression. *Cell Metab* **29**, 1376-1389 e1374, doi:10.1016/j.cmet.2019.02.016 (2019).

5 Noy, R. & Pollard, J. W. Tumor-associated macrophages: from mechanisms to therapy. *Immunity* **41**, 49-61, doi:10.1016/j.immuni.2014.06.010 (2014).

6 Rafii, S., Butler, J. M. & Ding, B. S. Angiocrine functions of organ-specific endothelial cells. *Nature* **529**, 316-325, doi:10.1038/nature17040 (2016).

7 Augustin, H. G. & Koh, G. Y. Organotypic vasculature: From descriptive heterogeneity to functional pathophysiology. *Science* **357**, doi:10.1126/science.aal2379 (2017).

8 Alsina-Sanchis, E., Mulfarth, R. & Fischer, A. Control of Tumor Progression by Angiocrine Factors. *Cancers (Basel)* **13**, doi:10.3390/cancers13112610 (2021).

9 Zhao, Q. *et al.* Single-Cell Transcriptome Analyses Reveal Endothelial Cell Heterogeneity in Tumors and Changes following Antiangiogenic Treatment. *Cancer Res* **78**, 2370-2382, doi:10.1158/0008-5472.CAN-17-2728 (2018).

10 Zhao, Q. *et al.* Heterogeneity and chimerism of endothelial cells revealed by single-cell transcriptome in orthotopic liver tumors. *Angiogenesis* **23**, 581-597, doi:10.1007/s10456-020-09727-9 (2020).

11 Wieland, E. *et al.* Endothelial Notch1 Activity Facilitates Metastasis. *Cancer Cell* **31**, 355-367, doi:10.1016/j.ccell.2017.01.007 (2017).

12 Bray, S. J. Notch signalling in context. *Nat Rev Mol Cell Biol* **17**, 722-735, doi:10.1038/nrm.2016.94 (2016).

13 Limbourg, F. P. *et al.* Essential role of endothelial Notch1 in angiogenesis. *Circulation* **111**, 1826-1832, doi:10.1161/01.CIR.0000160870.93058.DD (2005).

14 Hasan, S. S. *et al.* Endothelial Notch signaling controls insulin transport in muscle. *EMBO Mol Med* **12**, e09271, doi:10.15252/emmm.201809271 (2020).

15 Ramasamy, S. K., Kusumbe, A. P., Wang, L. & Adams, R. H. Endothelial Notch activity promotes angiogenesis and osteogenesis in bone. *Nature* **507**, 376-380, doi:10.1038/nature13146 (2014).

16 Sorensen, I., Adams, R. H. & Gossler, A. DLL1-mediated Notch activation regulates endothelial identity in mouse fetal arteries. *Blood* **113**, 5680-5688, doi:10.1182/blood-2008-08-174508 (2009).

17 Jabs, M. *et al.* Inhibition of Endothelial Notch Signaling Impairs Fatty Acid Transport and Leads to Metabolic and Vascular Remodeling of the Adult Heart. *Circulation* **137**, 2592-2608, doi:10.1161/CIRCULATIONAHA.117.029733 (2018).

18 Zhu, T. S. *et al.* Endothelial cells create a stem cell niche in glioblastoma by providing NOTCH ligands that nurture self-renewal of cancer stem-like cells. *Cancer Res* **71**, 6061-6072, doi:10.1158/0008-5472.CAN-10-4269 (2011).

19 Etzerodt, A. *et al.* Tissue-resident macrophages in omentum promote metastatic spread of ovarian cancer. *J Exp Med* **217**, doi:10.1084/jem.20191869 (2020).

20 Verginelli, F. *et al.* Activation of an endothelial Notch1-Jagged1 circuit induces VCAM1 expression, an effect amplified by interleukin-1beta. *Oncotarget* **6**, 43216-43229, doi:10.18632/oncotarget.6456 (2015).

21 Jablonska, J., Wu, C. F., Andzinski, L., Leschner, S. & Weiss, S. CXCR2-mediated tumor-associated neutrophil recruitment is regulated by IFN-beta. *Int J Cancer* **134**, 1346-1358, doi:10.1002/ijc.28551 (2014).

22 Taki, M. *et al.* Snail promotes ovarian cancer progression by recruiting myeloid-derived suppressor cells via CXCR2 ligand upregulation. *Nat Commun* **9**, 1685, doi:10.1038/s41467-018-03966-7 (2018).

23 Gilliver, S. C., Emmerson, E., Bernhagen, J. & Hardman, M. J. MIF: a key player in cutaneous biology and wound healing. *Exp Dermatol* **20**, 1-6, doi:10.1111/j.1600-0625.2010.01194.x (2011).

24 Alban, T. J. *et al.* Glioblastoma Myeloid-Derived Suppressor Cell Subsets Express Differential Macrophage Migration Inhibitory Factor Receptor Profiles That Can Be Targeted to Reduce Immune Suppression. *Front Immunol* **11**, 1191, doi:10.3389/fimmu.2020.01191 (2020).

25 Shi, X. *et al.* CD44 is the signaling component of the macrophage migration inhibitory factor-CD74 receptor complex. *Immunity* **25**, 595-606, doi:10.1016/j.immuni.2006.08.020 (2006).

26 Priego, N. *et al.* STAT3 labels a subpopulation of reactive astrocytes required for brain metastasis. *Nat Med* **24**, 1024-1035, doi:10.1038/s41591-018-0044-4 (2018).

27 Cortes, M. *et al.* Tumor-associated macrophages (TAMs) depend on ZEB1 for their cancer-promoting roles. *EMBO J* **36**, 3336-3355, doi:10.15252/embj.201797345 (2017).

28 Figueiredo, C. R. *et al.* Blockade of MIF-CD74 Signalling on Macrophages and Dendritic Cells Restores the Antitumour Immune Response Against Metastatic Melanoma. *Front Immunol* **9**, 1132, doi:10.3389/fimmu.2018.01132 (2018).

29 Przybyl, L. *et al.* CD74-Downregulation of Placental Macrophage-Trophoblastic Interactions in Preeclampsia. *Circ Res* **119**, 55-68, doi:10.1161/CIRCRESAHA.116.308304 (2016).

30 Moughon, D. L. *et al.* Macrophage Blockade Using CSF1R Inhibitors Reverses the Vascular Leakage Underlying Malignant Ascites in Late-Stage Epithelial Ovarian Cancer. *Cancer Res* **75**, 4742-4752, doi:10.1158/0008-5472.CAN-14-3373 (2015).

31 Zhang, F., Jiang, J., Xu, B., Xu, Y. & Wu, C. Over-expression of CXCL2 is associated with poor prognosis in patients with ovarian cancer. *Medicine (Baltimore)* **100**, e24125, doi:10.1097/MD.0000000000024125 (2021).

32 Di Mitri, D. *et al.* Re-education of Tumor-Associated Macrophages by CXCR2 Blockade Drives Senescence and Tumor Inhibition in Advanced Prostate Cancer. *Cell Rep* **28**, 2156-2168 e2155, doi:10.1016/j.celrep.2019.07.068 (2019).

33 Henriques, T. B. *et al.* Inhibition of CXCR2 plays a pivotal role in re-sensitizing ovarian cancer to cisplatin treatment. *Aging (Albany NY)* **13**, 13405-13420, doi:10.18632/aging.203074 (2021).

34 Alsina-Sanchis, E. *et al.* Intraperitoneal Oil Application Causes Local Inflammation with Depletion of Resident Peritoneal Macrophages. *Mol Cancer Res* **19**, 288-300, doi:10.1158/1541-7786.MCR-20-0650 (2021).

35 Sanjana, N. E., Shalem, O. & Zhang, F. Improved vectors and genome-wide libraries for CRISPR screening. *Nat Methods* **11**, 783-784, doi:10.1038/nmeth.3047 (2014).

36 Lake, R. J., Tsai, P. F., Choi, I., Won, K. J. & Fan, H. Y. RBPJ, the major transcriptional effector of Notch signaling, remains associated with chromatin throughout mitosis, suggesting a role in mitotic bookmarking. *PLoS Genet* **10**, e1004204, doi:10.1371/journal.pgen.1004204 (2014).

37 Szklarczyk, D. *et al.* The STRING database in 2021: customizable protein-protein networks, and functional characterization of user-uploaded gene/measurement sets. *Nucleic Acids Res* **49**, D605-D612, doi:10.1093/nar/gkaa1074 (2021).

38 Subramanian, A. *et al.* Gene set enrichment analysis: a knowledge-based approach for interpreting genome-wide expression profiles. *Proc Natl Acad Sci U S A* **102**, 15545-15550, doi:10.1073/pnas.0506580102 (2005).

39 de Vos van Steenwijk, P. J. *et al.* Tumor-infiltrating CD14-positive myeloid cells and CD8-positive T-cells prolong survival in patients with cervical carcinoma. *Int J Cancer* **133**, 2884-2894, doi:10.1002/ijc.28309 (2013).

Figure Legends

Figure 1. Reduced tumour burden in omentum and peritoneum of *Rbpj*$^{i\Delta EC}$ mice.

a, Model for the spread and proliferation of epithelial ovarian cancer (EOC) cells in the omentum. **b,** Schematic illustration of oral tamoxifen administration and metastatic EOC protocol. **c,** Representative pictures of ID8 tumour-bearing mouse omentum and microscopic images of omentum stained with H&E. Asterisk indicates pancreas. Scale bar, 2 mm. **d,** Representative images of immunohistochemistry staining for CD31 (white) and DAPI (blue) in omentum of ID8 tumour-bearing *Rbpj*$^{i\Delta EC}$ and control mice. At four weeks after tumour injection. Scale bar, 50 µm. Quantification of vessel density. Bar graphs show mean±SD; two-tailed, Welch's corrected t-test. **e,** Representative images of immunohistochemistry DAB cytokeratin (brown) staining. Scale bar, 20 µm. Tumour burden quantification of control (n=12) and *Rbpj*$^{i\Delta EC}$ mice (n=9). Bar graphs show mean±SD; two-tailed, Welch's corrected t-test **f**, Luciferase activity in peritoneal cavity of tumour-bearing *Rbpj*$^{i\Delta EC}$ compared to control mice four weeks after tumour injection. Quantification of luciferase levels in control (n=12) and *Rbpj*$^{i\Delta EC}$ (n=10). Bar graphs show mean±SD; two-tailed, Welch's corrected t-test.

Figure 2: Reduced MN-derived macrophage recruitment in metastatic EOC of *Rbpj*$^{i\Delta EC}$ mice.

a, Representative images of whole mount staining of tumour nodules of the omentum for luciferase (red), CD45 (green) and DAPI (blue) four weeks after tumour injection in *Rbpj*$^{i\Delta EC}$ and control mice. Scale bar, 20µm. Quantification of infiltrating immune cells (CD45$^+$) into tumour nodules (luciferase$^+$). Bar graphs show mean±SD; two-tailed, unpaired Mann-Whitney U-test. **b**, Representative images of tumour infiltrating myeloid cells, CD11b$^+$ (pink) in tumour areas, cytokeratin (brown) from *Rbpj*$^{i\Delta EC}$ and control mice four weeks after tumour injection. Scale bar, 50 µm. Quantification of CD11b$^+$ infiltrating cells area normalized by tumour area. Bar graphs show mean±SD; two-tailed, Welch's corrected t-test. Analysis of

myeloid cells within the peritoneal cavity after four weeks of tumour growth of *Rbpj*$^{i\Delta EC}$ and control mice by flow cytometry. Percentage of **c,** myeloid cells (CD45^{+}, CD11b^{high}) and **d,** macrophages (CD45^{+}, CD11b^{high}, F4/80^{+}) relative to alive cells. Bar graphs show mean±SD; two-tailed, unpaired Mann-Whitney U-test. **e,** Representative flow cytometer plot of monocyte-derived macrophages characterization by F4/80 and MHCII expression into LPM, IntPM and SPM in *Rbpj*$^{i\Delta EC}$ mice compared to controls and their quantification. Bar graphs show mean±SD; two-tailed, unpaired Mann-Whitney U-test. **f,** Quantification of newly recruited monocyte-derived macrophages (Tim4^{-} CCR2^{+}). Bar graphs show mean±SD; two-tailed, unpaired Mann-Whitney U-test. **g,** Scheme of transwell assay with human CD14^{+} monocyte through a monolayer of human umbilical vein endothelial cells (HUVECs) towards human ovarian cancer cells (SK-OV-3). **h**, Analysis of cell tracer carboxyfluorescein succinimidyl ester (CFSE) stained migrated CD14^{+} monocyte through monolayer of HUVECs with *RBPJ* KO and their representative images. Bar graphs show mean±SD; two-tailed, T-student's t-test.

Figure 3. Endothelial Notch-meditated recruitment via CXCL2.

a, Quantification of mRNA expression of CCL1, CCL21, CXCL12, and CXCL2 upon N1ICD overexpression, knock-out of *RBPJ* or their combination in HUVECs. Bar graphs show n-fold vs GFP transduced as mean±SD; two-tailed, unpaired Mann-Whitney U-test. **b,** Quantification of mRNA expression in whole peritoneal fat tissue from *Rbpj*$^{i\Delta EC}$ and control mice. Bar graphs show mean±SD; two-tailed, unpaired Mann-Whitney U-test. **c,** Quantification of mRNA expression in whole peritoneal fat tissue from ecN1ICD and control mice. Bar graphs show mean±SD; two-tailed, unpaired Mann-Whitney U-test. **d,** Scheme of RBPJ binding in *CXCL2* promotor region in murine and human genes. **e,** Enzyme-linked immunosorbent assay (ELISA) of CXCL2 of cell culture supernatant from HUVECs infected with N1ICD and GFP as control. Bar graphs show mean ±SD; two-tailed, unpaired Mann-Whitney U-test. **f,** Analysis of cell tracer carboxyfluorescein succinimidyl ester (CFSE)

stained migrated $CD14^+$ monocyte towards CXCL2 cytokine. Bar graphs show mean±SD; two-tailed, unpaired Mann-Whitney U-test. **g** ELISA of CXCL2 of HUVECs with knock down of *CXCL2*. Bar graphs show mean±SD; two-tailed, unpaired Mann-Whitney U-test. **h** Scheme of transwell assay with human $CD14^+$ monocyte through a monolayer of human umbilical vein endothelial cells (HUVECs) towards human ovarian cancer cells (SK-OV-3). Analysis of cell tracer carboxyfluorescein succinimidyl ester (CFSE) stained migrated $CD14^+$ monocyte through monolayer of HUVECs with knock down of CXCL2. Bar graphs show mean±SD; two-tailed, T-student's t-test.

Figure 4. Essential role of endothelial rbpj for tumour-mediated TAM education.

a, Schematic illustration of sorting of newly recruited monocyte-derived macrophages for microarray analysis after four weeks of tumour growth in *Rbpj*$^{i\Delta EC}$ and control mice. **b,** Gene set enrichment analysis (GSEA) of the tumour associated-macrophages (TAM) signature in recruited macrophages from *Rbpj*$^{i\Delta EC}$ vs. control mice compared with 20 most differentially regulated genes. **c**, Ingenuity pathways analysis (IPA) for upstream regulator in recruited macrophages from *Rbpj*$^{i\Delta EC}$ and control mice. Analysis of significant differentially regulated pathways by **d**, ingenuity pathways (IPA) and **e**, pathway analysis. **f**, GSEA of cholesterol homeostasis in recruited macrophages from *Rbpj*$^{i\Delta EC}$ vs. control mice with 20 most differentially regulated genes. **g**, Mean fluorescence intensity (MFI) of CD44 expression of human monocytes co-cultured with human ECs carrying an *RBPJ* knock-out. Bar graphs show mean ±SD; two-tailed, unpaired Mann-Whitney U-test. Quantification relative to control from Bone marrow-derived macrophages (BMDMs) after stimulation with conditioned medium from immortalized mouse cardiac ECs (MCECs) with *Rbpj* knock-out and control of **h**, *Cd44* and **i**, *Mmp9* mRNA expression. Bar graphs show mean±SD; two-tailed, paired students T-test. **j**, Quantification of mRNA expression of *Cd44* from macrophages isolated from peritoneal lavage of *Rbpj*$^{i\Delta EC}$ mice after 24 hours of thioglycollate i.p. injection relative to control. Bar graphs show mean±SD; two-tailed, unpaired students T-test. **k**, BMDMs control

and stimulated with CXCL2 (40ng/ml) for 72 hours. Quantification of mRNA expression of *CD44* relative to control. Bar graphs show mean±SD; two-tailed, paired students T-test. **l**, Representative images of BMDMs stained with CD44 (white), CD45 (red) and DAPI (blue) of control and stimulated with CXCL2 (40ng/ml) for 72 hours.

Figure 5. CXCL2 expression in ovarian cancer patients correlates with CD44 expression and TAM education.

a, Analysis of *CD44* raw counts in $CXCL2^{hi}$ (n=97) vs $CXCl2^{low}$ (n=100) patient stratification of publicly available bulk tumour of human ovarian cancer from the Cancer Genome Atlas (TCGA) database using R Studio software. Bar graphs show median; two-tailed, unpaired T-student's t-test. **b**, GSEA of the tumour associated-macrophage (TAM) signature in $CXCL2^{low}$ vs. $CXCL2^{high}$ ovarian cancer patients from the TCGA database. Analysis of KEGG pathways of **c,** $CXCL2^{low}$ and **d,** $CXCL2^{high}$ patients fold changes and shown as Log2-ratio from extracted p-values. **e**, GSEA of cholesterol homeostasis in $CXCL2^{low}$ vs. $CXCL2^{high}$ ovarian cancer patients from the TCGA database.

Figure 6. Loss of endothelial *Rbpj* increases cytotoxic potential and proportion of cytotoxic T cells in peritoneal lavage of tumour-bearing mice.

a, *In silico* protein-protein interaction analysis shows the association between CXCR2, CD44 and CD74. Results were mapped with CXCR2 as query protein using the STRING database. Protein-protein results are obtained using medium confidence interaction score (0.400). Line thickness of network edges indicates the strength of data support. **b,** GSEA of publicly available data (E-MTAB-3309) of TAM signature in WT vs. CD74 knock-out (KO) IL-4-treated BMDMs with 10 most differentially regulated gene extracted from. **c**, GSEA of CD74-mediated gene signature in recruited macrophages from $Rbpj^{i\Delta EC}$ vs. control mice with 10 most differentially regulated genes. **d**, Schematic illustration of T cell sorting for cytotoxicity

assay after six weeks of tumour growth. **e**, Lactate dehydrogenase (LDH)-cytotoxicity assay of sorted $CD3^+$ T cells and incubation with *in vitro* cultivated murine ovarian cancer cells (ID8) measured by absorbance at 450nm including blank correction. Bar graphs show mean±SD; two-tailed, unpaired Mann-Whitney U-test. **f,** Percentage of $CD3^+$ cells (relative to $CD45^+$ cells) and their proportion in $CD4^+$ and $CD8^+$ T cells (relative to $CD3^+$ cells) in peritoneal lavage of *Rbpj*$^{i\Delta EC}$ and control mice 4 weeks after tumour injection. Bar graphs show mean±SD; two-tailed, unpaired Mann-Whitney U-test. **g,** Model of endothelial Notch1-dependent recruitment and education of MN-derived macrophages (TAM) into the tumour microenvironment. Tumour cells (TC) activate Notch1 on the tumour endothelium. Activation of endothelial Notch signalling leads to a secretion of angiocrine factors, especially CXCL2, which leads to an increased infiltration of monocyte-derived macrophages (by its receptor CXCR2) into the tumour microenvironment. Loss of endothelial Notch signalling inhibits TC-induced education of TAMs by priming of monocytes (MN) leading to a downregulation of hyaluronan receptor, CD44 as well as pro-tumorigenic receptor CD74 on TAMs. Model created with BioRender.com.

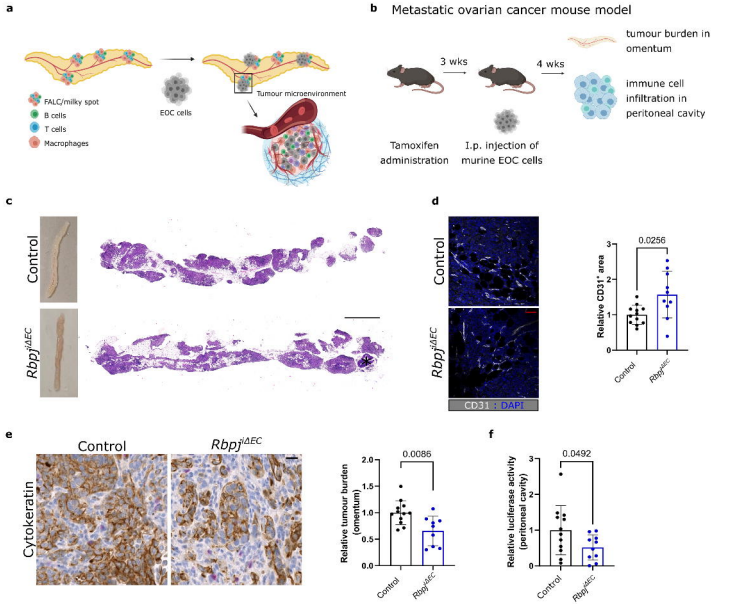
a
FALC/milky spot
B cells
T cells
Macrophages
EOC cells
Tumour microenvironment
b
Metastatic ovarian cancer mouse model
3 wks
4 wks
tumour burden in omentum
immune cell infiltration in peritoneal cavity
Tamoxifen administration
I.p. injection of murine EOC cells
c
Control
Rbpj^iΔEC
d
Control
Rbpj^iΔEC
CD31 : DAPI
Relative CD31+ area
0.0256
Control
Rbpj^iΔEC
e
Control
Rbpj^iΔEC
Cytokeratin
Relative tumour burden (omentum)
0.0086
Control
Rbpj^iΔEC
f
Relative luciferase activity (peritoneal cavity)
0.0492
Control
Rbpj^iΔEC

Figure 1.

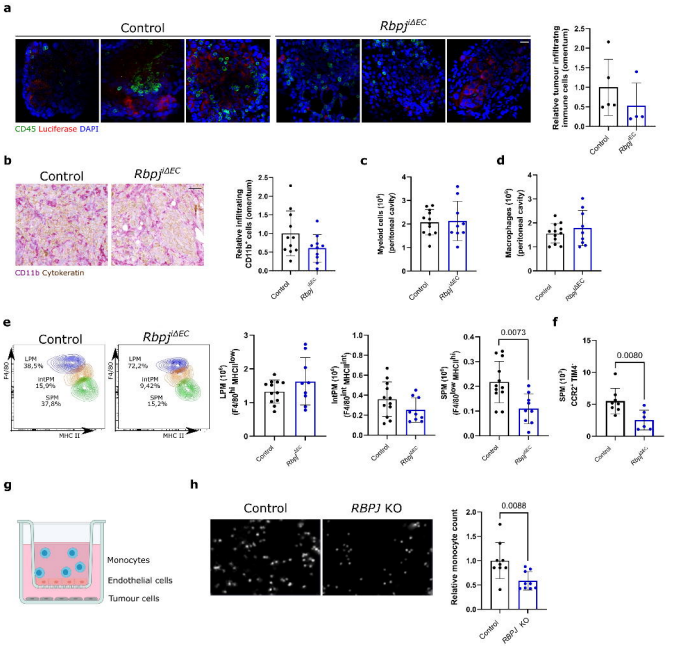
a
Control
RbpjiΔEC
CD45 Luciferase DAPI
Relative tumour infiltrating immune cells (area/mm²)
Control
RbpjiΔEC
b
Control
RbpjiΔEC
CD11b Cytokeratin
Relative infiltrating CD11b+ cells (area/mm)
c
Myeloid cells (10⁶) (peritoneal cavity)
d
Macrophages (10⁶) (peritoneal cavity)
e
Control
RbpjiΔEC
LPM 38,5%
IntPM 15,9%
SPM 37,8%
LPM 72,2%
IntPM 9,42%
SPM 15,2%
F4/80
MHC II
LPM (10⁷) (F4/80hi MHCIIhi)
IntPM (10⁷) (F4/80int MHCIIint)
SPM (10⁷) (F4/80int MHCIIhi)
0.0073
f
SPM (10⁷) CCR2+ TIM4+
0.0080
g
Monocytes
Endothelial cells
Tumour cells
h
Control
RBPJ KO
Relative monocyte count
0.0088

Figure 2.

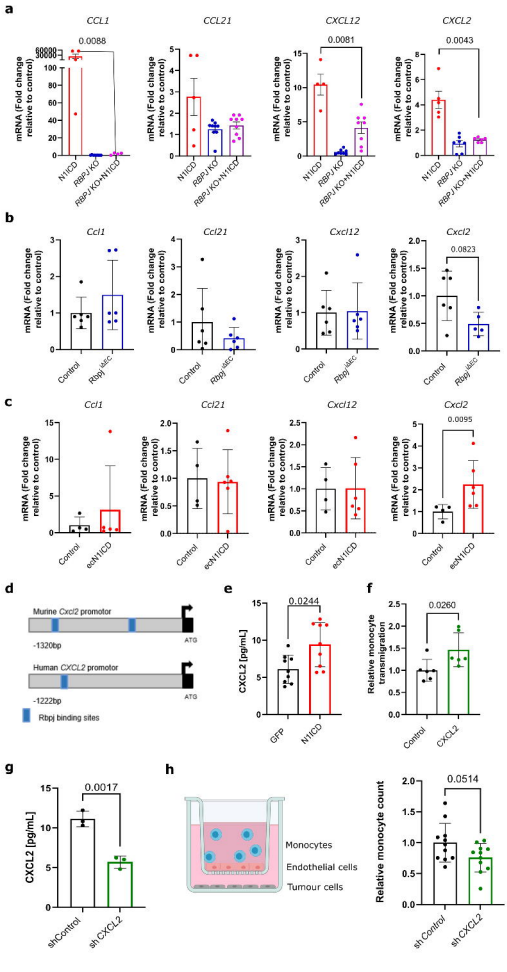
a
CCL1
CCL21
CXCL12
CXCL2
0.0088
0.0081
0.0043
mRNA (Fold change relative to control)
N1ICD
RBPJ KO
RBPJ KO+N1ICD
b
Ccl1
Ccl21
Cxcl12
Cxcl2
0.0823
Control
Rbpj iMEC
c
0.0095
ecN1ICD
d
Murine Cxcl2 promotor
-1320bp
ATG
Human CXCL2 promotor
-1222bp
Rbpj binding sites
e
CXCL2 [pg/mL]
0.0244
GFP
f
Relative monocyte transmigration
0.0260
CXCL2
g
0.0017
shControl
shCXCL2
h
Monocytes
Endothelial cells
Tumour cells
Relative monocyte count
0.0514
sh.Control
shCXCL2

Figure 3.

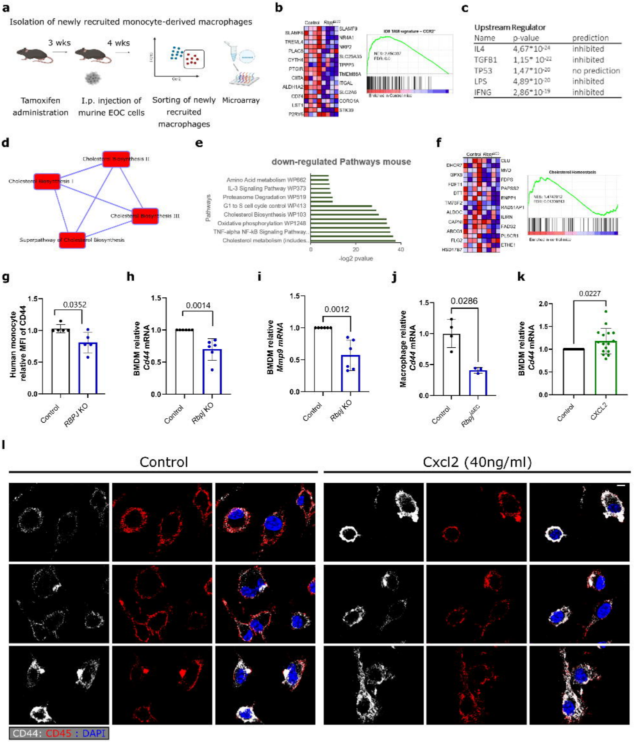
a
Isolation of newly recruited monocyte-derived macrophages
3 wks
4 wks
Tamoxifen administration
I.p. injection of murine EOC cells
Sorting of newly recruited macrophages
Microarray
b
c
Upstream Regulator
Name p-value prediction
IL4 4,67*10-24 inhibited
TGFB1 1,15*10-22 inhibited
TP53 1,47*10-20 no prediction
LPS 4,89*10-20 inhibited
IFNG 2,86*10-19 inhibited
d
Cholesterol Biosynthesis I
Cholesterol Biosynthesis II
Cholesterol Biosynthesis III
Superpathway of Cholesterol Biosynthesis
e
down-regulated Pathways mouse
Amino Acid metabolism WP662
IL-3 Signaling Pathway WP373
Proteasome Degradation WP519
G1 to S cell cycle control WP413
Cholesterol Biosynthesis WP103
Oxidative phosphorylation WP1248
Pathways
-log2 pvalue
f
g
Human monocyte relative MFI of CD44
0.0352
Control
RBPJ KO
h
BMDM relative Cd44 mRNA
0.0014
Control
Rbpj KO
i
BMDM relative Mmp9 mRNA
0.0012
Control
Rbpj KO
j
Macrophage relative Cd44 mRNA
0.0286
Control
k
BMDM relative Cd44 mRNA
0.0227
Control
CXCL2
l
Control
Cxcl2 (40ng/ml)
CD44: CD45 : DAPI

Figure 4.

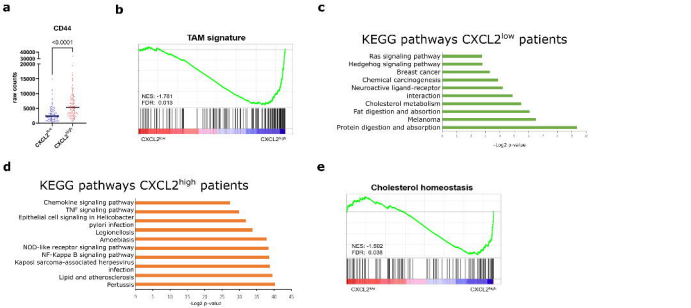
a
CD44
<0.0001
raw counts
CXCL2low
CXCL2high
b
TAM signature
NES: -1.781
FDR: 0.010
CXCL2low
CXCL2high
c
KEGG pathways CXCL2low patients
Ras signaling pathway
Hedgehog signaling pathway
Breast cancer
Chemical carcinogenesis
Neuroactive ligand-receptor interaction
Cholesterol metabolism
Fat digestion and absorption
Melanoma
Protein digestion and absorption
-Log2 p-value
d
KEGG pathways CXCL2high patients
Chemokine signaling pathway
TNF signaling pathway
Epithelial cell signaling in Helicobacter pylori infection
Legionellosis
Amoebiasis
NOD-like receptor signaling pathway
NF-Kappa B signaling pathway
Kaposi sarcoma-associated herpesvirus infection
Lipid and atherosclerosis
Pertussis
-Log2 p-value
e
Cholesterol homeostasis
NES: -1.592
FDR: 0.038
CXCL2low
CXCL2high

Figure 5.

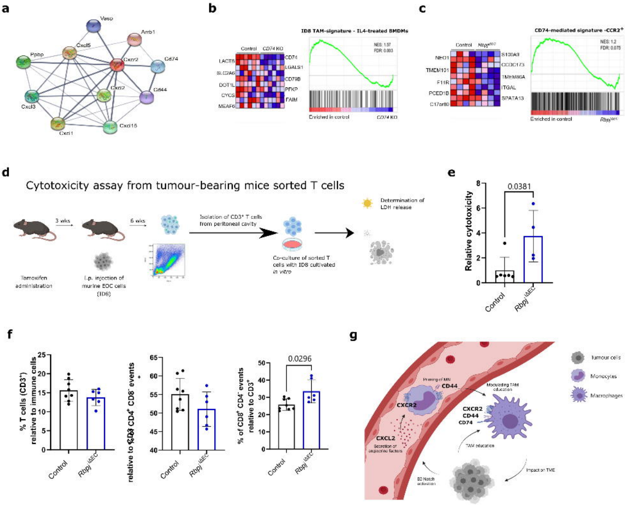
a
Vasp
Arrb1
Cxcl5
Ppbp
Cxcr2
Cd74
Cxcl2
Cd44
Cxcl3
Cxcl1
Cxcl15
b
ID8 TAM-signature - IL4-treated BMDMs
Control
CD74 KO
NES: 1.57
FDR: 0.003
LACTB
SLC2A6
DOT1L
CYCS
MEAF6
CD74
LGALS1
CD79B
PFKP
FAIM
Enriched in control
CD74 KO
c
CD74-mediated signature -CCR2+
Control
NES: 1.2
FDR: 0.075
NEO1
TMEM101
F11R
PCED1B
C17orf80
S100A9
CCDC173
TMEM86A
ITGAL
SPATA13
Enriched in control
d
Cytotoxicity assay from tumour-bearing mice sorted T cells
3 wks
6 wks
Isolation of CD3+ T cells from peritoneal cavity
Determination of LDH release
Tamoxifen administration
i.p. injection of murine EOC cells (ID8)
Co-culture of sorted T cells with ID8 cultivated in vitro
e
Relative cytotoxicity
0.0381
Control
Rbpj iΔEC
f
% T cells (CD3+) relative to immune cells
relative to % CD3 CD4+ CD8- events
% of CD8+ CD4- events relative to CD3+
0.0296
Control
Rbpj iΔEC
g
Tumour cells
Monocytes
Macrophages
Priming of MN
CD44
Modulating TAM education
CXCR2
CXCR2
CD44
CD74
CXCL2
Secretion of angiocrine factors
TAM education
Impact on TME
EC Notch activation

Figure 6.